

CaesarNeRF: Calibrated Semantic Representation for Few-Shot Generalizable Neural Rendering

Haidong Zhu^{1,*}Tianyu Ding^{2,*†}Tianyi Chen²Ilya Zharkov²Ram Nevatia¹Luming Liang^{2,†}¹University of Southern California²Microsoft

{haidongz, nevatia}@usc.edu, {tianyuding, tiachen, zharkov, lulian}@microsoft.com

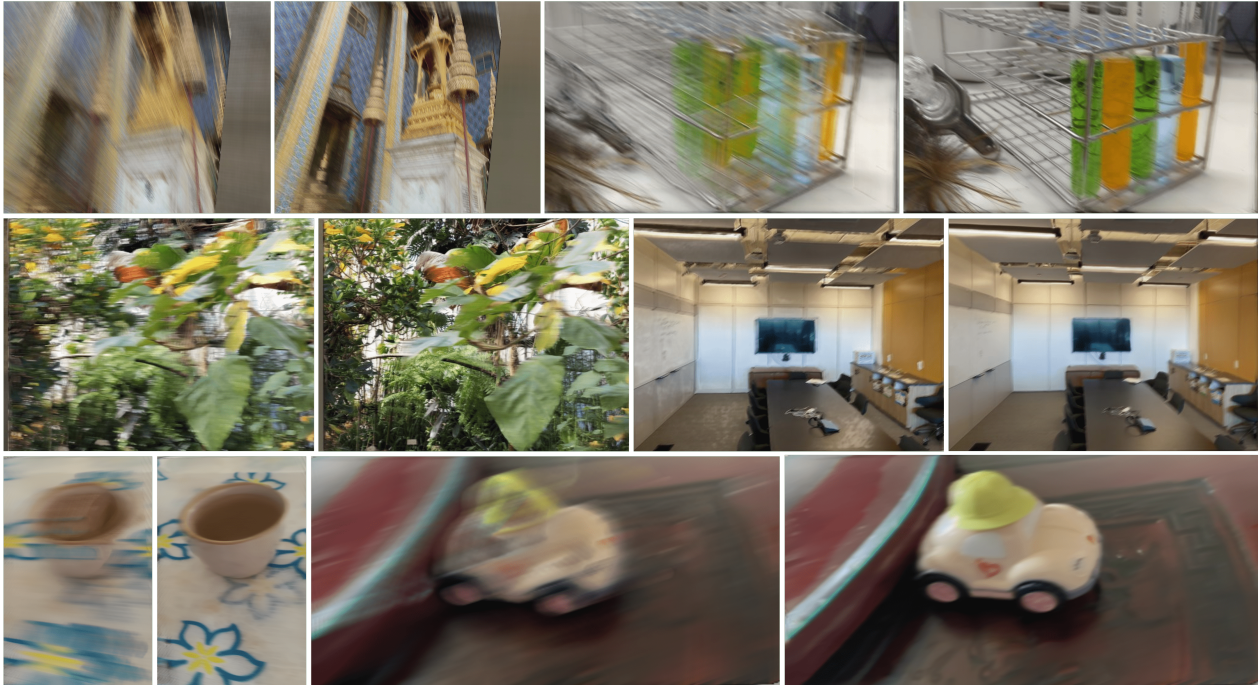


Figure 1. Novel view synthesis for novel scenes using **ONE** reference view on Shiny [59], LLFF [36], and MVIImgNet [68] (top to bottom). Each pair of images corresponds to the results from GNT [52] (left) and CaesarNeRF (right).

Abstract

Generalizability and few-shot learning are key challenges in Neural Radiance Fields (NeRF), often due to the lack of a holistic understanding in pixel-level rendering. We introduce CaesarNeRF, an end-to-end approach that leverages scene-level CALibratEd SemAntic Representation along with pixel-level representations to advance few-shot, generalizable neural rendering, facilitating a holistic understanding without compromising high-quality details. CaesarNeRF explicitly models pose differences of reference views to combine scene-level semantic representations, providing a calibrated holistic understand-

ing. This calibration process aligns various viewpoints with precise location and is further enhanced by sequential refinement to capture varying details. Extensive experiments on public datasets, including LLFF, Shiny, mip-NeRF 360, and MVIImgNet, show that CaesarNeRF delivers state-of-the-art performance across varying numbers of reference views, proving effective even with a single reference image. The project page of this work can be found [here](#).

1. Introduction

Rendering a scene from a novel camera position is essential in view synthesis [5, 11, 54]. The recent advancement of Neural Radiance Field (NeRF) [38] has shown impressive

*Equal contribution.

†Corresponding author.

results in creating photo-realistic images from novel viewpoints. However, conventional NeRF methods are either typically scene-specific, necessitating retraining for novel scenes [15, 16, 38, 59, 65], or require a large number of reference views as input for generalizing to novel scenarios [6, 50, 52, 67]. These constraints highlight the complexity of the few-shot generalizable neural rendering, which aims to render unseen scenes from novel viewpoints with a limited number of reference images.

Generalizing NeRF to novel scenes often involves using pixel-level feature embeddings encoded from input images, as seen in existing methods [51, 67]. These methods adapt NeRF to novel scenes by separating the scene representation from the model through an image encoder. However, relying solely on pixel-level features has its drawbacks: it requires highly precise epipolar geometry and often overlooks occlusion in complex scenes. Moreover, employing pixel-level features ignores the inherent interconnections within objects in the scene, treating the prediction of each pixel independently. This becomes problematic with a limited number of input reference images, as the data scarcity amplifies prediction ambiguity, significantly influenced by the biases of the input camera views.

We present CaesarNeRF, a method that advances the generalizability of NeRF by incorporating calibrated semantic representation. This enables rendering from novel viewpoints using as few as one input reference view, as depicted in Figure 1. Our approach combines semantic scene-level representation with per-pixel features, enhancing consistency across different views of the same scene. The encoder-generated scene-level representations capture both semantic features and biases linked to specific camera poses. When reference views are limited, these biases can introduce uncertainty in the rendered images. To counter this, CaesarNeRF integrates camera pose transformations into the semantic representation, hence the term *calibrated*. By isolating pose-specific information from the scene-level representation, our model harmonizes features across input views, mitigating view-specific biases and, in turn, reducing ambiguity. In addition, CaesarNeRF introduces a sequential refinement process, which equips the model with varying levels of detail needed to enhance the semantic features. Extensive experiments on datasets such as LLFF [36], Shiny [59], mip-NeRF 360 [4], and the newly released MVIImgNet [68] demonstrate that CaesarNeRF outperforms current state-of-the-art methods, proving effective in generalizable settings with as few as one reference view.

In summary, our contributions are as follows:

- We introduce CaesarNeRF, which utilizes scene-level calibrated semantic representation to achieve few-shot, generalizable neural rendering. This innovation leads to coherent and high-quality renderings.
- We integrate semantic scene context with pixel-level de-

tails, in contrast to existing methods that rely solely on pixel-level features. We also address view-specific biases by modeling camera pose transformations and enhance the scene understanding through the sequential refinement of semantic features.

- We demonstrate through extensive experiments that CaesarNeRF consistently outperforms state-of-the-art generalizable NeRF methods across a variety of datasets. Furthermore, integrating the Caesar pipeline into other baseline methods leads to consistent performance gains, highlighting its effectiveness and adaptability.

2. Related work

Neural Radiance Field (NeRF) implicitly captures the density and appearance of points within a scene or object [37, 38] and enable rendering from novel camera positions. In recent years, NeRF has witnessed improvements in a wide range of applications, such as photo-realistic novel view synthesis for large-scale scenes [34, 60, 71], dynamic scene decomposition and deformation [21, 27, 31, 40–42, 44, 75, 76], occupancy or depth estimation [58, 62, 74], scene generation and editing [1, 20, 28, 30, 35, 43, 63, 64, 70], and so on. Despite these advances, most methods still rely on the original NeRF and require retraining or fine-tuning for novel scenes not covered in the training data.

Generalizable NeRF aims to adapt a single NeRF model to multiple scenes by separating the scene representation from the model. This field has seen notable advancements, with efforts focused on avoiding the need for retraining [8, 18, 33, 56, 57, 66, 67]. PixelNeRF [67] and GRF [51] pioneered the application of an image encoder to transform images into per-pixel features, with NeRF functioning as a decoder for predicting density and color from these features. MVSNeRF [6] introduces the use of a cost volume from MVSNet [66] to encode 3-D features from multiple views. Recognizing the intrinsic connection between points along a ray, IBRNet [56] employs self-attention to enhance point density predictions. Transformer-based [53] networks like GNT [10, 52], GeoNeRF [22], and GPNR [50] are explored as alternatives to volume rendering, concentrating on pixel and patch-level representations. Additionally, InsertNeRF [2] utilizes hypernet modules to adapt parameters for novel scenes efficiently.

These methods primarily depend on image encoders to extract pixel-aligned features from reference views. As a result, many of them lack a comprehensive understanding of the entire scene. Furthermore, with few reference views, the features become intertwined with view-specific details, compromising the quality of the rendering results.

Few-shot Neural Radiance Field aims to render novel views using a limited number of reference images. To this end, various methods have been developed, incorporating additional information such as normalization-flow [69], se-

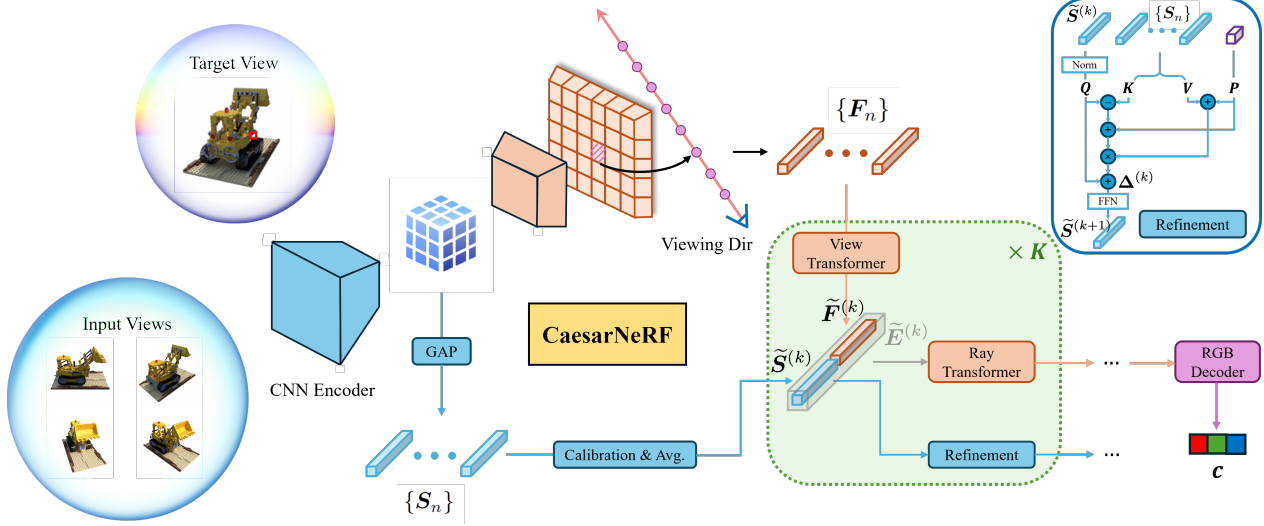


Figure 2. Overview of CaesarNeRF. CaesarNeRF employs a shared encoder to capture two types of features from input views, including scene-level semantic representation $\{S_n\}$ and pixel-level feature representation $\{F_n\}$. Following calibration and aggregation of $\{S_n\}$ from various views, we concatenate it with the pixel-level fused feature, processed by the view transformer. Subsequent use of the ray-transformer, coupled with sequential refinement, enables us to render the final RGB values for each pixel in the target view.

mantic constraints [17, 19], depth cues [13, 46], geometry consistency [3, 26, 39, 55, 61], and frequency content [65]. Others [6, 9] emphasize pretraining on large-scale datasets.

While these methods offer reasonable reconstructions with few inputs, they typically still require training or fine-tuning for specific scenes. Moreover, these methods usually require at least three reference images. With fewer than three, view-specific biases lead to ambiguity, complicating the rendering. Diffusion-based [12, 32, 49, 73] and other generative methods [24, 77] have been explored for single-view synthesis or generative rendering, yet they are mostly limited to single-object rendering and generally fall short for complex scenes, which often result in a style change as shown in the supplementary material.

CaesarNeRF confronts the above challenges by leveraging calibrated semantic representations that exploit scene geometry and variations in camera viewpoints. As a result, CaesarNeRF overcomes the limitations of pixel-level features and reduces dependency on external data or extensive pretraining, delivering high-quality renderings in few-shot and generalizable settings.

3. The proposed method

We first outline the general framework of existing generalizable NeRF in Section 3.1. Then, we present our proposed CaesarNeRF, as illustrated in Figure 2. This model integrates elements of semantic representation, calibration, and sequential refinement, detailed in Section 3.2, 3.3, and 3.4, respectively. The training objective is given in Section 3.5.

3.1. NeRF and generalizable NeRF

Neural Radiance Field (NeRF) [37, 38] aims to render 3D scenes by predicting both the density and RGB values at points where light rays intersect the radiance field. For a query point $x \in \mathbb{R}^3$ and a viewing direction d on the unit sphere \mathbb{S}^2 in 3D space, the NeRF model \mathcal{F} is defined as:

$$\sigma, c = \mathcal{F}(x, d). \quad (1)$$

Here, $\sigma \in \mathbb{R}$ and $c \in \mathbb{R}^3$ denote the density and the RGB values, respectively. After computing these values for a collection of discretized points along each ray, volume rendering techniques are employed to calculate the final RGB values for each pixel, thus reconstructing the image.

However, traditional NeRF models \mathcal{F} are limited by their requirement for scene-specific training, making it unsuitable for generalizing to novel scenes. To overcome this, generalizable NeRF models, denoted by \mathcal{F}_G , are designed to render images of novel scenes without per-scene training. Given N reference images $\{I_n\}_{n=1}^N$, an encoder-based generalizable NeRF model \mathcal{F}_G decouples the object representation from the original NeRF by using an encoder to extract per-pixel feature maps $\{F_n\}_{n=1}^N$ from the input images. To synthesize a pixel associated with a point x along a ray in direction d , it projects $\{F_n\}_{n=1}^N$ from nearby views and aggregates this multi-view pixel-level information using techniques such as average pooling [67] or cost volumes [6]. This results in a fused feature embedding \tilde{F} , allowing \mathcal{F}_G to predict density σ and RGB values c for each point along

the ray, as expressed by:

$$\sigma, c = \mathcal{F}_G(x, d, \tilde{\mathbf{F}}). \quad (2)$$

In our method, we adopt the recently introduced fully attention-based generalizable NeRF method, GNT [52], as both the backbone and the baseline. GNT shares a similar paradigm with (2) but employs transformers [53] to aggregate pixel-level features into $\tilde{\mathbf{F}}$. It uses a *view transformer* to fuse projected pixel-level features from reference views, and a *ray transformer* to combine features from different points along a ray, eliminating the need for volume rendering. Further details about GNT can be found in [52]. We also demonstrate that our approach can be extended to other generalizable NeRF models, as discussed in Section 4.2.

3.2. Scene-level semantic representation

Both encoder-based generalizable NeRF models [6, 51, 67] and their attention-based counterparts [50, 52] mainly rely on pixel-level feature representations. While effective, this approach restricts their capability for a holistic scene understanding, especially when reference views are scarce. This limitation also exacerbates challenges in resolving depth ambiguities between points along the rays, a problem that becomes more pronounced with fewer reference views.

To address these challenges, we introduce semantic representations aimed at enriching the scene-level understanding. We utilize a shared CNN encoder and apply a Global Average Pooling (GAP) to its C -dimensional output feature map, generating N global feature vectors $\{\mathbf{S}_n\}_{n=1}^N$ corresponding to each input view. These feature vectors are then averaged to form a unified scene-level representation \mathbf{S} , *i.e.*,

$$\mathbf{S} = \frac{1}{N} \sum_{n=1}^N \mathbf{S}_n \in \mathbb{R}^C. \quad (3)$$

In GNT [52], which uses a view transformer to aggregate pixel-level features into an L -dimensional vector $\tilde{\mathbf{F}}$, we extend this by concatenating $\tilde{\mathbf{F}}$ with \mathbf{S} to construct a *global-local* embedding \mathbf{E} , as formulated by:

$$\mathbf{E} = \text{Concat}(\tilde{\mathbf{F}}, \mathbf{S}) \in \mathbb{R}^{L+C}. \quad (4)$$

This combined embedding \mathbf{E} is then subjected to the standard self-attention mechanism used in GNT [52]. This approach enables the scene-level semantic representation (\mathbf{S}) to integrate with per-point features ($\tilde{\mathbf{F}}$), offering a more nuanced understanding at both levels. It also allows each point to selectively draw from the scene-level information. To maintain dimensional consistency across the input and output layers of multiple transformer modules, we employ a two-layer MLP to project the enhanced features back to the original dimension L of the per-point embedding $\tilde{\mathbf{F}}$.

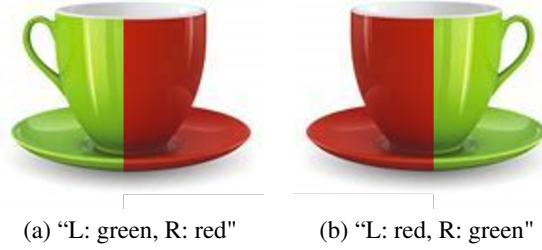


Figure 3. An illustration of conflicting semantic meanings from multiple viewpoints of the same object. When observing the cup from distinct angles, the features retain spatial information but are inconsistent in the scene-level semantic understanding.

3.3. Calibration of semantic representation

The integration of the scene-level semantic representation \mathbf{S} , generated through simple averaging of global feature vectors as in (3), improves rendering quality. However, this approach has limitations when dealing with multiple views. As illustrated in Figure 3, viewing the same object from distinct angles may retain spatial attributes but can lead to conflicting semantic meanings. Merely averaging these global feature vectors without accounting for camera positions can result in a distorted scene-level understanding.

To mitigate this inconsistency, we propose a semantic calibration technique using feature rotation. This adjustment aligns the semantic representation across different camera poses. Our inspiration comes from the use of camera pose projection in computing the fused pixel-level feature $\tilde{\mathbf{F}}$ and is further motivated by [45], which demonstrates that explicit rotation operations in feature spaces are feasible. Unlike point clouds in [45] that inherently lack a defined canonical orientation, NeRF explicitly encodes differences between camera viewpoints, thereby enabling precise calibration between the reference and target images.

Building on this observation, we calculate calibrated semantic representations $\{\tilde{\mathbf{S}}_n\}_{n=1}^N$ from the N original semantic representations $\{\mathbf{S}_n\}_{n=1}^N$ derived from the reference views. We accomplish this by leveraging their respective rotation matrices $\{\mathbf{T}_n\}_{n=1}^N$ to model the rotational variations between each input view and the target view. The alignment of the original semantic features is performed as follows:

$$\tilde{\mathbf{S}}_n = \mathcal{P}(\mathbf{T}_n \cdot \mathcal{P}^{-1}(\mathbf{S}_n)), \text{ where } \mathbf{T}_n = \mathbf{T}_{\text{out}}^{\text{w2c}} \cdot \mathbf{T}_n^{\text{c2w}}. \quad (5)$$

Here, $\mathbf{T}_n^{\text{c2w}}$ is the inverse of the extrinsic matrix used for \mathbf{I}_n , and $\mathbf{T}_{\text{out}}^{\text{w2c}}$ is the extrinsic matrix for the target view. $\mathcal{P}(\cdot)$ and $\mathcal{P}^{-1}(\cdot)$ are the flattening and inverse flattening operations, which reshape the feature to a 1D vector of shape 1-by- C and a 2D matrix of shape 3-by- $\frac{C}{3}$, respectively.

Note that for the extrinsic matrix, we consider only the top-left 3×3 submatrix that accounts for rotation. Using GAP to condense feature maps of various sizes into a 1-by-



Figure 4. Visualization of decoded feature maps for “orchid” in LLFF dataset, produced by *ray transformers* [52] at different stages. From left to right, the transformer stages increase in depth.

C feature vector eliminates the need for scaling parameters in the semantic representation. As a result, modeling the intrinsic matrix is unnecessary, assuming no skewing, making our approach adaptable to different camera configurations.

With the calibrated semantic features $\{\tilde{S}_n\}_{n=1}^N$ for each reference view, we average these, similar to (3), to obtain the calibrated scene-level semantic representation \tilde{S} , *i.e.*,

$$\tilde{S} = \frac{1}{N} \sum_{n=1}^N \tilde{S}_n \in \mathbb{R}^C. \quad (6)$$

Finally, akin to (4), we concatenate the pixel-level fused feature \tilde{F} with the calibrated scene-level semantic representation \tilde{S} to form the final global-local embedding \tilde{E} :

$$\tilde{E} = \text{Concat}(\tilde{F}, \tilde{S}) \in \mathbb{R}^{L+C}. \quad (7)$$

This unified embedding then feeds into ray transformers, passing through standard self-attention mechanisms. In the original GNT [52], multiple view transformers and ray transformers are stacked alternately for sequential feature processing. The last ray transformer integrates features from multiple points along a ray to yield the final RGB value. We denote the corresponding feature representations at stage k as $\tilde{F}^{(k)}$ and $\tilde{E}^{(k)}$. Notably, the calibrated semantic representation \tilde{S} remains constant across these stages.

3.4. Sequential refinement

While leveraging \tilde{S} improves consistency, a single, uniform \tilde{S} may not be adequate for deeper layers that demand more nuanced details. In fact, we find that deeper transformers capture finer details compared to shallower ones, as shown in Figure 4. To address this limitation, we introduce a sequential semantic feature refinement module that progressively enriches features at each stage. Specifically, we learn the residual $\Delta^{(k)}$ to update \tilde{S} at each stage k as follows:

$$\tilde{S}^{(k+1)} \leftarrow \tilde{S}^{(k)} + \Delta^{(k)}. \quad (8)$$

Here, $\Delta^{(k)}$ is calculated by first performing specialized cross-attentions between $\tilde{S}^{(k)}$ and the original, uncalibrated per-frame semantic features $\{S_n\}_{n=1}^N$ (see Figure 2), followed by their summation. Our goal is to fuse information from different source views to enrich the scene-level

semantic representation with features from each reference frame. With this sequential refinement, we combine $\tilde{S}^{(k)}$ with $\tilde{F}^{(k)}$ at each stage, yielding a stage-specific global-local embedding $\tilde{E}^{(k)}$, which completes our approach.

Discussion. In scenarios with few reference views, especially when limited to just one, the primary issue is inaccurate depth estimation, resulting in depth ambiguity [12]. This compromises the quality of images when rendered from novel viewpoints. Despite this, essential visual information generally remains accurate across different camera poses. Incorporating our proposed scene-level representation improves the understanding of the overall scene layout [7], distinguishing our approach from existing generalizable NeRF models that predict pixels individually. The advantage of our approach is its holistic view; the semantic representation enriches per-pixel predictions by providing broader context. This semantic constraint ensures that fewer abrupt changes between adjacent points. Consequently, it leads to more reliable depth estimations, making the images rendered from limited reference views more plausible.

3.5. Training objectives

During training, we employ three different loss functions:

MSE loss. The Mean Square Error (MSE) loss is the standard photometric loss used in NeRF [37]. It computes the MSE between the actual and predicted pixel values.

Central loss. To ensure frame-wise calibrated semantic features $\{\tilde{S}_n\}_{n=1}^N$ are consistent when projected onto the same target view, we introduce a central loss, defined as:

$$\mathcal{L}_{\text{central}} = \frac{1}{N} \sum_{n=1}^N \|\tilde{S}_n - \tilde{S}\|_1. \quad (9)$$

Point-wise perceptual loss. During the rendering of a bath of pixels in a target view, we inpaint the ground-truth image by replacing the corresponding pixels with the predicted ones. Then, a perceptual loss [23] is computed between the inpainted image and the target image to guide the training process at the whole-image level.

The final loss function is formulated as follows:

$$\mathcal{L} = \mathcal{L}_{\text{MSE}} + \lambda_1 \mathcal{L}_{\text{central}} + \lambda_2 \mathcal{L}_{\text{perc}}. \quad (10)$$

Empirically, we set $\lambda_1 = 1$ and $\lambda_2 = 0.001$, following [29].

4. Experiments

4.1. Experimental setups

For the experimental setups, we begin by describing the datasets used in our experiments. This is followed by implementation details of our proposed method and the baseline methods we employed for comparison.

Input	Method	PSNR (\uparrow)	LPIPS (\downarrow)	SSIM (\uparrow)
1-view	PixelNeRF [67]	9.32	0.898	0.264
	GPNR [50]	15.91	0.527	0.400
	NeuRay [33]	16.18	0.584	0.393
	IBRNet [56]	16.85	0.542	0.507
	GNT [52]	16.57	0.500	0.424
	Ours	18.31	0.435	0.521
2-view	PixelNeRF [67]	11.23	0.766	0.282
	GPNR [50]	18.79	0.380	0.575
	NeuRay [33]	17.71	0.336	0.646
	GeoNeRF [22]	18.76	0.473	0.500
	MatchNeRF [8]	21.08	0.272	0.689
	MVSNeRF [6]	19.15	0.336	0.704
	IBRNet [56]	21.25	0.333	0.685
	GNT [52]	20.88	0.251	0.691
3-view	Ours	21.94	0.224	0.736
	PixelNeRF [67]	11.24	0.671	0.486
	GPNR [50]	21.57	0.288	0.695
	NeuRay [33]	18.26	0.310	0.672
	GeoNeRF [22]	23.40	0.246	0.766
	MatchNeRF [8]	22.30	0.234	0.731
	MVSNeRF [6]	19.84	0.314	0.729
	IBRNet [56]	23.00	0.262	0.752
4-view	GNT [52]	23.21	0.178	0.782
	Ours	23.45	0.176	0.794

Table 1. Results for generalizable scene rendering on LLFF with few reference views. GeoNeRF, MatchNeRF, and MVSNeRF necessitate variance as input, defaulting to 0 for single-image cases, hence their results are not included for 1-view scenarios.

Datasets. Firstly, following [52], we construct our training data from both synthetic and real data. This collection includes scanned models from Google Scanned Objects [14], RealEstate10K [72], and handheld phone captures [56]. For evaluation, we utilize real data encompassing complex scenes from sources such as LLFF [36], Shiny [59], and mip-NeRF 360 [4]. Additionally, we train and test our model using the recently released MVImgNet dataset [68]. We adhere to the official split, focusing on examples from the *containers* category, and select 2,500 scenes for training. During inference, we choose 100 scenes, using their first images as target views and the spatially nearest images as references. Since MVImgNet does not provide camera poses, we utilize COLMAP [47, 48] to deduce the camera positions within these scenes.

Implementation details. CaesarNeRF is built upon GNT [52], for which we maintain the same configuration, setting the *ray* and *view* transformers stack number (K) to 8 for generalizable setting and 4 for single-scene setting. The feature encoder extracts bottleneck features, applies GAP, and then uses a fully connected (FC) layer to reduce the input dimension C to 96. Training involves 500,000 iterations using the Adam optimizer [25], with learning rate set at 0.001 for the feature encoder and 0.0005 for CaesarNeRF, halving them every 100,000 iterations. Each iteration samples 4,096 rays from a single scene. In line with [52],

Input	Method	PSNR (\uparrow)	LPIPS (\downarrow)	SSIM (\uparrow)
1-view	IBRNet [56]	14.93	0.625	0.401
	GNT [52]	15.99	0.548	0.400
	Ours	17.57	0.467	0.472
2-view	MatchNeRF [8]	20.28	0.278	0.636
	MVSNeRF [6]	17.25	0.416	0.577
	IBRNet [56]	18.40	0.400	0.595
3-view	GNT [52]	20.42	0.327	0.617
	Ours	21.47	0.293	0.652
	MatchNeRF [8]	20.77	0.249	0.672
4-view	MVSNeRF [6]	18.55	0.343	0.645
	IBRNet [56]	21.96	0.281	0.710
	GNT [52]	22.47	0.247	0.720
5-view	Ours	22.74	0.241	0.723

Table 2. Results for generalizable scene rendering on Shiny with few reference views.

Input	Method	PSNR (\uparrow)	LPIPS (\downarrow)	SSIM (\uparrow)
1-view	IBRNet [56]	14.12	0.682	0.283
	GNT [52]	13.48	0.630	0.314
	Ours	15.20	0.592	0.350
2-view	MatchNeRF [8]	17.00	0.566	0.392
	MVSNeRF [6]	14.23	0.681	0.366
	IBRNet [56]	16.24	0.618	0.360
3-view	GNT [52]	15.21	0.559	0.370
	Ours	17.05	0.538	0.403
	MatchNeRF [8]	17.26	0.551	0.407
4-view	MVSNeRF [6]	14.29	0.674	0.406
	IBRNet [56]	17.70	0.555	0.420
	GNT [52]	15.59	0.538	0.395
5-view	Ours	17.55	0.512	0.430

Table 3. Results for generalizable scene rendering on mip-NeRF 360 with few reference views.

we randomly choose between 8 to 10 reference views for training, and 3 to 7 views when using the MVImgNet [68].

Baseline methods. We compare CaesarNeRF with several state-of-the-art methods suited for generalizable NeRF applications, including earlier works such as MVS-NeRF [6], PixelNeRF [67], and IBRNet [56], alongside more recent ones, including GPNR [50], NeuRay [33], GNT [52], GeoNeRF [22] and MatchNeRF [8].

4.2. Results and analysis

We compare results in two settings: a generalizable setting, where the model is trained on multiple scenes without fine-tuning during inference for both few and all reference view cases, and a single-scene setting where the model is trained and evaluated on just one scene. Following these comparisons, we conduct ablation studies and test the generalizability of our method with other state-of-the-art approaches.

Generalizable rendering. In the generalizable setting, we adopt two training strategies. First, we train the model on multiple datasets as described in Section 4.1 and eval-

		PSNR (\uparrow)	LPIPS (\downarrow)	SSIM (\uparrow)
1-view	IBRNet	19.14	0.458	0.595
	GN	22.22	0.433	0.678
	Ours w/o C.	23.61	0.371	0.718
	Ours	24.28	0.334	0.747
2-view	IBRNet	24.38	0.266	0.818
	GN	26.94	0.236	0.850
	Ours w/o C.	26.34	0.274	0.817
	Ours	27.34	0.215	0.856
3-view	IBRNet	25.53	0.203	0.858
	GN	27.41	0.206	0.870
	Ours w/o C.	27.10	0.228	0.850
	Ours	27.82	0.190	0.875
4-view	IBRNet	25.99	0.190	0.867
	GN	27.51	0.197	0.875
	Ours w/o C.	27.30	0.210	0.862
	Ours	27.92	0.181	0.881
5-view	IBRNet	26.12	0.188	0.867
	GN	27.51	0.194	0.876
	Ours w/o C.	27.34	0.203	0.865
	Ours	27.92	0.179	0.882

Table 4. Results on MVImgNet across varying numbers of reference views. ‘C.’ represents the use of calibration before averaging.

uate on LLFF [36], Shiny [59] and mip-NeRF 360 [4] datasets. In addition, the model is trained and tested on the MVImgNet [68] for object-centric generalizability.

(a) **LLFF, Shiny, and mip-NeRF 360.** The results for few-reference view scenarios on these datasets are shown in Tables 1, 2 and 3, respectively. Methods like Match-NeRF [8], MVSNeRF [66], and GeoNeRF [22] require at least two reference views. On the LLFF dataset, all methods experience a performance decline as the number of views decreases. CaesarNeRF, however, consistently outperforms others across varying reference view numbers, with the performance gap becoming more significant with fewer views. For example, with 3 views, while IBRNet [56] and GNT [52] have comparable PSNRs, CaesarNeRF demonstrates a more substantial lead in LPIPS and SSIM metrics.

Similar patterns are observed on the Shiny [59] and mip-NeRF 360 [4] datasets. We apply the highest-performing methods from the LLFF evaluations and report the results for those that produce satisfactory outcomes with few reference views. CaesarNeRF maintains superior performance throughout. Notably, for complex datasets like mip-NeRF 360 [4], which have sparse camera inputs, the quality of rendered images generally decreases with fewer available reference views. Nonetheless, CaesarNeRF shows the most robust performance compared to the other methods.

(b) **MVImgNet.** We extend our comparison of CaesarNeRF with GNT [52] and IBRNet [56] on the MVImgNet dataset, focusing on object-centric scenes, as shown in Table 4. We examine a variant of CaesarNeRF where semantic

Method	PSNR (\uparrow)	LPIPS (\downarrow)	SSIM (\uparrow)
LLFF [36]	23.27	0.212	0.798
NeRF [38]	26.50	0.250	0.811
NeX [59]	27.26	0.179	0.904
GNT [52]	27.24	0.087	0.889
Ours	27.64	0.081	0.904

Table 5. Results of per-scene optimization on LLFF, in comparison with state-of-the-art methods.

Method	Input	PSNR (\uparrow)	SSIM (\uparrow)	LPIPS (\downarrow)
MatchNeRF [8]	2-view	20.59	0.775	0.276
	3-view	22.43	0.805	0.244
Caesar-MatchNeRF	2-view	21.55	0.782	0.268
	3-view	22.98	0.824	0.242
IBRNet [56]	1-view	16.85	0.507	0.542
	2-view	21.25	0.685	0.333
	3-view	23.00	0.752	0.262
Caesar-IBRNet	1-view	17.76	0.543	0.500
	2-view	22.39	0.740	0.275
	3-view	23.67	0.772	0.242

Table 6. Results on LLFF for few-shot generalization after adapting Caesar to other baseline methods.

Model Variations		PSNR (\uparrow)	LPIPS (\downarrow)	SSIM (\uparrow)
R len.	Seq.	Cali.		
		(Baseline GNT)	20.93	0.185
				0.731
Ext.			20.85	0.173
+32			21.43	0.152
+64			21.49	0.149
+96			21.46	0.150
+128			21.49	0.147
+ 96	✓		21.53	0.146
+ 96		✓	21.51	0.147
+ 96	✓	✓	21.67	0.139
				0.781

Table 7. Ablations on the semantic representation length R , sequential refinement (Seq.) and calibration (Cali.). ‘Ext.’ denotes the extension of per-pixel representation to a length of 64 in GNT.

calibration is substituted with simple feature averaging from multiple frames. While the performance of all methods improves with more views, CaesarNeRF consistently outperforms GNT and IBRNet. Notably, CaesarNeRF with feature averaging surpasses GNT in 1-view case but lags with additional views, implying that the absence of calibration lead to ambiguities when rendering from multiple views.

Per-scene optimization. Beyond the multi-scene generalizable setting, we demonstrate per-scene optimization results in Table 5. Testing across 8 categories from the LLFF dataset [36], we calculate the average performance over these scenes. CaesarNeRF consistently outperforms nearly all state-of-the-art methods in the comparison, across

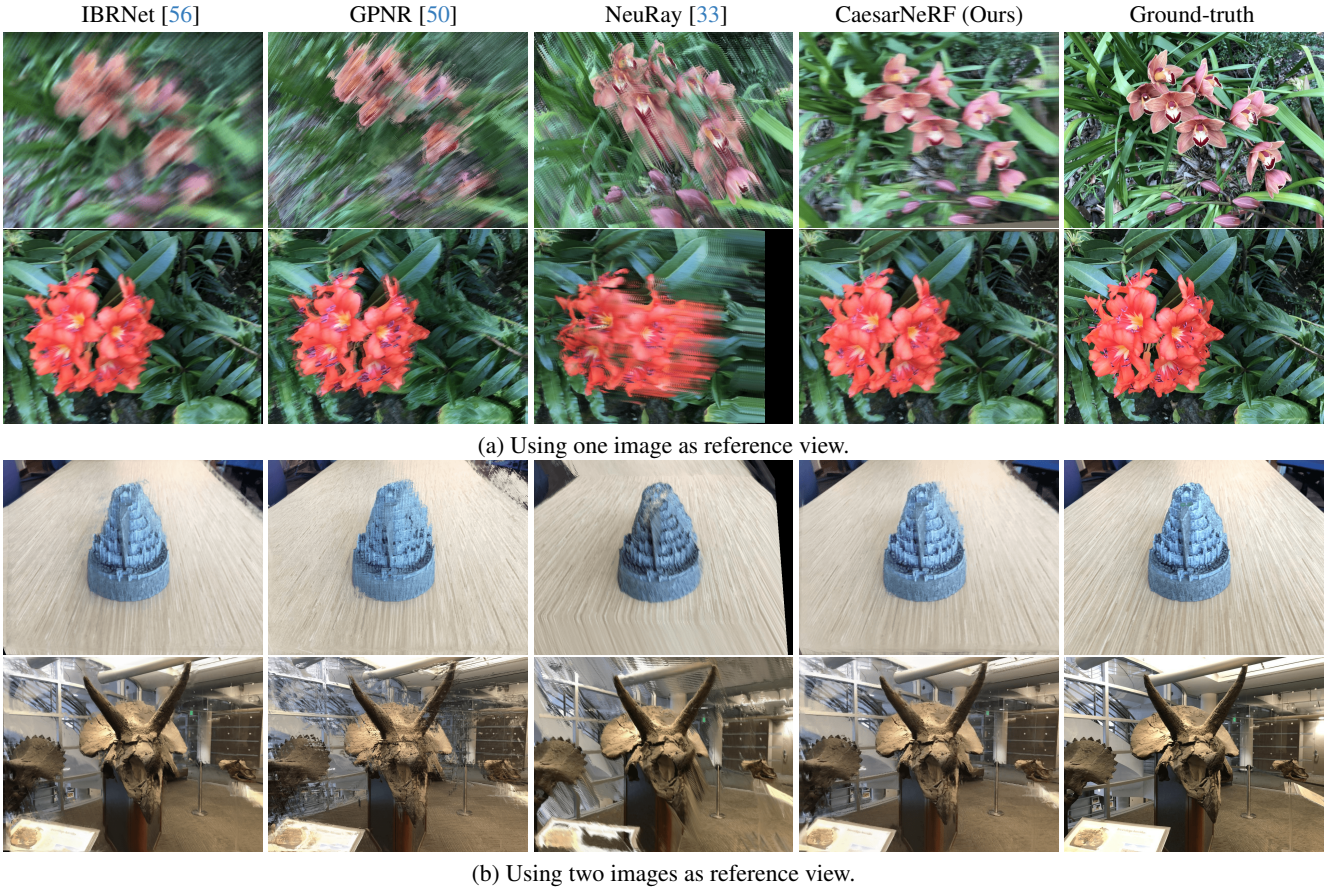


Figure 5. Comparative visualization of our proposed method against other state-of-the-art methods.

all three metrics, showing a significant improvement over our baseline method, GNT [52].

Adaptability. To test the adaptability of our Caesar pipeline, we apply it to two other state-of-the-art methods that use *view transformers*, namely MatchNeRF [8] and IBRNet [56]. We demonstrate in Table 6 that our enhancements in scene-level semantic understanding significantly boost the performance of these methods across all metrics. This indicates that the Caesar framework is not only beneficial in our CaesarNeRF, which is based on GNT [52], but can also be a versatile addition to other NeRF pipelines.

Ablation analysis. We conduct ablation studies on the “orchid” scene from the LLFF dataset, with findings detailed in Table 7. Testing variations in representation and the impact of the sequential refinement and calibration modules, we find that increasing the latent size in GNT yields marginal benefits. However, incorporating even a modest semantic representation size distinctly improves results. The length of the semantic representation has a minimal impact on quality. Our ablation studies indicate that while sequential refinement and calibration each offer slight perfor-

mance gains, their combined effect is most significant. In a single-scene context, semantic information is effectively embedded within the representation, making the benefits of individual modules subtler. Together, however, they provide a framework where sequential refinement can leverage calibrated features for deeper insights.

Visualizations. We present our visualization results in Figure 5, where we compare our method with others using one or two views from the LLFF dataset. Additional visual comparisons are provided in the supplementary materials. These visualizations highlight that in scenarios with few views, our method significantly surpasses the competitors, particularly excelling when only a single view is available. In such cases, CaesarNeRF demonstrates enhanced clarity, with sharper boundaries and more distinct objects.

5. Conclusion and limitation

In this paper, we introduce CaesarNeRF, a few-shot and generalizable NeRF pipeline that combines scene-level semantic with per-pixel feature representations, aiding in rendering from novel camera positions with limited reference

views. We calibrate the semantic representations across different input views and employ a sequential refinement network to offer distinct semantic representations at various levels. Our method has been extensively evaluated on a broad range of datasets, exhibiting state-of-the-art performance in both generalizable and single-scene settings.

Limitations. CaesarNeRF could be further improved by integrating explicit depth information and generative capabilities, which could provide a richer basis for rendering from novel views with few reference images.

References

- [1] Chong Bao, Yinda Zhang, Bangbang Yang, Tianxing Fan, Zesong Yang, Hujun Bao, Guofeng Zhang, and Zhaopeng Cui. Sine: Semantic-driven image-based nerf editing with prior-guided editing field. In *CVPR*, pages 20919–20929, 2023. [2](#)
- [2] Yanqi Bao, Tianyu Ding, Jing Huo, Wenbin Li, Yuxin Li, and Yang Gao. Insertnerf: Instilling generalizability into nerf with hypernet modules. *arXiv preprint arXiv:2308.13897*, 2023. [2](#)
- [3] Yanqi Bao, Yuxin Li, Jing Huo, Tianyu Ding, Xinyue Liang, Wenbin Li, and Yang Gao. Where and how: Mitigating confusion in neural radiance fields from sparse inputs. *arXiv preprint arXiv:2308.02908*, 2023. [3](#)
- [4] Jonathan T Barron, Ben Mildenhall, Dor Verbin, Pratul P Srinivasan, and Peter Hedman. Mip-nerf 360: Unbounded anti-aliased neural radiance fields. In *CVPR*, pages 5470–5479, 2022. [2, 6, 7](#)
- [5] Chris Buehler, Michael Bosse, Leonard McMillan, Steven Gortler, and Michael Cohen. Unstructured lumigraph rendering. In *SIGGRAPH*, pages 425–432, 2001. [1](#)
- [6] Anpei Chen, Zexiang Xu, Fuqiang Zhao, Xiaoshuai Zhang, Fanbo Xiang, Jingyi Yu, and Hao Su. Mvsnerf: Fast generalizable radiance field reconstruction from multi-view stereo. In *ICCV*, pages 14124–14133, 2021. [2, 3, 4, 6](#)
- [7] Weihua Chen, Xianzhe Xu, Jian Jia, Hao Luo, Yaohua Wang, Fan Wang, Rong Jin, and Xiuyu Sun. Beyond appearance: a semantic controllable self-supervised learning framework for human-centric visual tasks. In *CVPR*, 2023. [5](#)
- [8] Yuedong Chen, Haofei Xu, Qianyi Wu, Chuanxia Zheng, Tat-Jen Cham, and Jianfei Cai. Explicit correspondence matching for generalizable neural radiance fields. *arXiv preprint arXiv:2304.12294*, 2023. [2, 6, 7, 8](#)
- [9] Julian Chibane, Aayush Bansal, Verica Lazova, and Gerard Pons-Moll. Stereo radiance fields (srf): Learning view synthesis for sparse views of novel scenes. In *CVPR*, pages 7911–7920, 2021. [3](#)
- [10] Wenyan Cong, Hanxue Liang, Peihao Wang, Zhiwen Fan, Tianlong Chen, Mukund Varma, Yi Wang, and Zhangyang Wang. Enhancing nerf akin to enhancing llms: Generalizable nerf transformer with mixture-of-view-experts. In *ICCV*, 2023. [2](#)
- [11] Paul E Debevec, Camillo J Taylor, and Jitendra Malik. Modeling and rendering architecture from photographs: A hybrid geometry-and image-based approach. In *SIGGRAPH*, pages 11–20, 1996. [1](#)
- [12] Congyue Deng, Chiyu “Max” Jiang, Charles R. Qi, Xinchen Yan, Yin Zhou, Leonidas Guibas, and Dragomir Anguelov. Nerdi: Single-view nerf synthesis with language-guided diffusion as general image priors. In *CVPR*, pages 20637–20647, 2023. [3, 5](#)
- [13] Kangle Deng, Andrew Liu, Jun-Yan Zhu, and Deva Ramanan. Depth-supervised nerf: Fewer views and faster training for free. In *CVPR*, pages 12882–12891, 2022. [3](#)
- [14] Laura Downs, Anthony Francis, Nate Koenig, Brandon Kinman, Ryan Hickman, Krista Reymann, Thomas B McHugh, and Vincent Vanhoucke. Google scanned objects: A high-quality dataset of 3d scanned household items. In *ICRA*, pages 2553–2560, 2022. [6](#)
- [15] Sara Fridovich-Keil, Giacomo Meanti, Frederik Rahbæk Warburg, Benjamin Recht, and Angjoo Kanazawa. K-planes: Explicit radiance fields in space, time, and appearance. In *CVPR*, pages 12479–12488, 2023. [2](#)
- [16] Yang Fu, Ishan Misra, and Xiaolong Wang. Multiplane nerf-supervised disentanglement of depth and camera pose from videos. In *ICML*, 2022. [2](#)
- [17] Yiming Gao, Yan-Pei Cao, and Ying Shan. Surfelnerf: Neural surfel radiance fields for online photorealistic reconstruction of indoor scenes. In *CVPR*, pages 108–118, 2023. [3](#)
- [18] Muhammad Zubair Irshad, Sergey Zakharov, Katherine Liu, Vitor Guizilini, Thomas Kollar, Adrien Gaidon, Zsolt Kira, and Rares Ambrus. Neo 360: Neural fields for sparse view synthesis of outdoor scenes. In *ICCV*, pages 9187–9198, 2023. [2](#)
- [19] Ajay Jain, Matthew Tancik, and Pieter Abbeel. Putting nerf on a diet: Semantically consistent few-shot view synthesis. In *ICCV*, pages 5885–5894, 2021. [3](#)
- [20] Ajay Jain, Ben Mildenhall, Jonathan T Barron, Pieter Abbeel, and Ben Poole. Zero-shot text-guided object generation with dream fields. In *CVPR*, pages 867–876, 2022. [2](#)
- [21] Yifan Jiang, Peter Hedman, Ben Mildenhall, Dejia Xu, Jonathan T Barron, Zhangyang Wang, and Tianfan Xue. Alignerf: High-fidelity neural radiance fields via alignment-aware training. In *CVPR*, pages 46–55, 2023. [2](#)
- [22] Mohammad Mahdi Johari, Yann Lepoittevin, and François Fleuret. Geonerf: Generalizing nerf with geometry priors. In *CVPR*, pages 18365–18375, 2022. [2, 6, 7](#)
- [23] Justin Johnson, Alexandre Alahi, and Li Fei-Fei. Perceptual losses for real-time style transfer and super-resolution. In *Computer Vision–ECCV 2016: 14th European Conference, Amsterdam, The Netherlands, October 11–14, 2016, Proceedings, Part II* 14, pages 694–711. Springer, 2016. [5](#)
- [24] Adam Kania, Artur Kasymov, Maciej Zięba, and Przemysław Spurek. Hypernerfgan: Hypernetwork approach to 3d nerf gan. *arXiv preprint arXiv:2301.11631*, 2023. [3](#)
- [25] Diederik P Kingma and Jimmy Ba. Adam: A method for stochastic optimization. *arXiv preprint arXiv:1412.6980*, 2014. [6](#)
- [26] Minseop Kwak, Jiuhn Song, and Seungryong Kim. Geconerf: Few-shot neural radiance fields via geometric consistency. *arXiv preprint arXiv:2301.10941*, 2023. [3](#)

- [27] Zhengqi Li, Qianqian Wang, Forrester Cole, Richard Tucker, and Noah Snavely. Dynibar: Neural dynamic image-based rendering. In *CVPR*, pages 4273–4284, 2023. 2
- [28] Chen-Hsuan Lin, Jun Gao, Luming Tang, Towaki Takikawa, Xiaohui Zeng, Xun Huang, Karsten Kreis, Sanja Fidler, Ming-Yu Liu, and Tsung-Yi Lin. Magic3d: High-resolution text-to-3d content creation. In *CVPR*, pages 300–309, 2023. 2
- [29] Haotong Lin, Sida Peng, Zhen Xu, Yunzhi Yan, Qing Shuai, Hujun Bao, and Xiaowei Zhou. Efficient neural radiance fields for interactive free-viewpoint video. In *SIGGRAPH Asia 2022 Conference Papers*, pages 1–9, 2022. 5
- [30] Yiqi Lin, Haotian Bai, Sijia Li, Haonan Lu, Xiaodong Lin, Hui Xiong, and Lin Wang. Componerf: Text-guided multi-object compositional nerf with editable 3d scene layout. *arXiv preprint arXiv:2303.13843*, 2023. 2
- [31] Lingjie Liu, Marc Habermann, Viktor Rudnev, Kripasindhu Sarkar, Jiatao Gu, and Christian Theobalt. Neural actor: Neural free-view synthesis of human actors with pose control. *TOC*, 40(6):1–16, 2021. 2
- [32] Ruoshi Liu, Rundi Wu, Basile Van Hoorick, Pavel Tokmakov, Sergey Zakharov, and Carl Vondrick. Zero-1-to-3: Zero-shot one image to 3d object. In *ICCV*, 2023. 3
- [33] Yuan Liu, Sida Peng, Lingjie Liu, Qianqian Wang, Peng Wang, Christian Theobalt, Xiaowei Zhou, and Wenping Wang. Neural rays for occlusion-aware image-based rendering. In *CVPR*, pages 7824–7833, 2022. 2, 6, 8
- [34] Ricardo Martin-Brualla, Noha Radwan, Mehdi SM Sajjadi, Jonathan T Barron, Alexey Dosovitskiy, and Daniel Duckworth. Nerf in the wild: Neural radiance fields for unconstrained photo collections. In *CVPR*, pages 7210–7219, 2021. 2
- [35] Gal Metzer, Elad Richardson, Or Patashnik, Raja Giryes, and Daniel Cohen-Or. Latent-nerf for shape-guided generation of 3d shapes and textures. In *CVPR*, pages 12663–12673, 2023. 2
- [36] Ben Mildenhall, Pratul P Srinivasan, Rodrigo Ortiz-Cayon, Nima Khademi Kalantari, Ravi Ramamoorthi, Ren Ng, and Abhishek Kar. Local light field fusion: Practical view synthesis with prescriptive sampling guidelines. *TOG*, 38(4):1–14, 2019. 1, 2, 6, 7
- [37] Ben Mildenhall, Pratul P. Srinivasan, Matthew Tancik, Jonathan T. Barron, Ravi Ramamoorthi, and Ren Ng. Nerf: Representing scenes as neural radiance fields for view synthesis. In *ECCV*, 2020. 2, 3, 5
- [38] Ben Mildenhall, Pratul P Srinivasan, Matthew Tancik, Jonathan T Barron, Ravi Ramamoorthi, and Ren Ng. Nerf: Representing scenes as neural radiance fields for view synthesis. *Communications of the ACM*, 65(1):99–106, 2021. 1, 2, 3, 7
- [39] Michael Niemeyer, Jonathan T Barron, Ben Mildenhall, Mehdi SM Sajjadi, Andreas Geiger, and Noha Radwan. Reg-nerf: Regularizing neural radiance fields for view synthesis from sparse inputs. In *CVPR*, pages 5480–5490, 2022. 3
- [40] Atsuhiro Noguchi, Xiao Sun, Stephen Lin, and Tatsuya Harada. Neural articulated radiance field. In *ICCV*, pages 5762–5772, 2021. 2
- [41] Keunhong Park, Utkarsh Sinha, Jonathan T Barron, Sofien Bouaziz, Dan B Goldman, Steven M Seitz, and Ricardo Martin-Brualla. Nerfies: Deformable neural radiance fields. In *ICCV*, pages 5865–5874, 2021.
- [42] Sida Peng, Junting Dong, Qianqian Wang, Shangzhan Zhang, Qing Shuai, Xiaowei Zhou, and Hujun Bao. Animatable neural radiance fields for modeling dynamic human bodies. In *ICCV*, pages 14314–14323, 2021. 2
- [43] Ben Poole, Ajay Jain, Jonathan T Barron, and Ben Mildenhall. Dreamfusion: Text-to-3d using 2d diffusion. *arXiv preprint arXiv:2209.14988*, 2022. 2
- [44] Albert Pumarola, Enric Corona, Gerard Pons-Moll, and Francesc Moreno-Noguer. D-nerf: Neural radiance fields for dynamic scenes. In *CVPR*, pages 10318–10327, 2021. 2
- [45] Charles R Qi, Hao Su, Kaichun Mo, and Leonidas J Guibas. Pointnet: Deep learning on point sets for 3d classification and segmentation. In *CVPR*, pages 652–660, 2017. 4
- [46] Barbara Roessle, Jonathan T Barron, Ben Mildenhall, Pratul P Srinivasan, and Matthias Nießner. Dense depth priors for neural radiance fields from sparse input views. In *CVPR*, pages 12892–12901, 2022. 3
- [47] Johannes Lutz Schönberger and Jan-Michael Frahm. Structure-from-motion revisited. In *CVPR*, 2016. 6
- [48] Johannes Lutz Schönberger, Enliang Zheng, Marc Pollefeys, and Jan-Michael Frahm. Pixelwise view selection for unstructured multi-view stereo. In *ECCV*, 2016. 6
- [49] J Ryan Shue, Eric Ryan Chan, Ryan Po, Zachary Ankner, Jiajun Wu, and Gordon Wetzstein. 3d neural field generation using triplane diffusion. In *CVPR*, pages 20875–20886, 2023. 3
- [50] Mohammed Suhail, Carlos Esteves, Leonid Sigal, and Ameesh Makadia. Generalizable patch-based neural rendering. In *ECCV*, pages 156–174, 2022. 2, 4, 6, 8
- [51] Alex Trevithick and Bo Yang. Grf: Learning a general radiance field for 3d representation and rendering. In *ICCV*, pages 15182–15192, 2021. 2, 4
- [52] Mukund Varma, Peihao Wang, Xuxi Chen, Tianlong Chen, Subhashini Venugopalan, and Zhangyang Wang. Is attention all that nerf needs? In *ICLR*, 2023. 1, 2, 4, 5, 6, 7, 8
- [53] Ashish Vaswani, Noam Shazeer, Niki Parmar, Jakob Uszkoreit, Llion Jones, Aidan N Gomez, Łukasz Kaiser, and Illia Polosukhin. Attention is all you need. *NeurIPS*, 30, 2017. 2, 4
- [54] Michael Waechter, Nils Moehrle, and Michael Goesele. Let there be color! large-scale texturing of 3d reconstructions. In *ECCV*, pages 836–850, 2014. 1
- [55] Guangcong Wang, Zhaoxi Chen, Chen Change Loy, and Ziwei Liu. Sparsenerf: Distilling depth ranking for few-shot novel view synthesis. In *ICCV*, 2023. 3
- [56] Qianqian Wang, Zhicheng Wang, Kyle Genova, Pratul P Srinivasan, Howard Zhou, Jonathan T Barron, Ricardo Martin-Brualla, Noah Snavely, and Thomas Funkhouser. Ibr-net: Learning multi-view image-based rendering. In *CVPR*, pages 4690–4699, 2021. 2, 6, 7, 8
- [57] Tengfei Wang, Bo Zhang, Ting Zhang, Shuyang Gu, Jianmin Bao, Tadas Baltrusaitis, Jingjing Shen, Dong Chen, Fang Wen, Qifeng Chen, et al. Rodin: A generative model for

- sculpting 3d digital avatars using diffusion. In *CVPR*, pages 4563–4573, 2023. 2
- [58] Yi Wei, Shaohui Liu, Yongming Rao, Wang Zhao, Jiwen Lu, and Jie Zhou. Nerfingmvs: Guided optimization of neural radiance fields for indoor multi-view stereo. In *CVPR*, pages 5610–5619, 2021. 2
- [59] Suttisak Wizadwongsu, Pakkapon Phongthawee, Jiraphon Yenphraphai, and Supasorn Suwajanakorn. Nex: Real-time view synthesis with neural basis expansion. In *CVPR*, pages 8534–8543, 2021. 1, 2, 6, 7
- [60] Yuanbo Xiangli, Lining Xu, Xingang Pan, Nanxuan Zhao, Anyi Rao, Christian Theobalt, Bo Dai, and Dahua Lin. Bungeenerf: Progressive neural radiance field for extreme multi-scale scene rendering. In *ECCV*, 2022. 2
- [61] Dejia Xu, Yifan Jiang, Peihao Wang, Zhiwen Fan, Humphrey Shi, and Zhangyang Wang. Sinnerf: Training neural radiance fields on complex scenes from a single image. In *ECCV*, pages 736–753, 2022. 3
- [62] Qiangeng Xu, Zexiang Xu, Julien Philip, Sai Bi, Zhixin Shu, Kalyan Sunkavalli, and Ulrich Neumann. Point-nerf: Point-based neural radiance fields. In *CVPR*, pages 5438–5448, 2022. 2
- [63] Bangbang Yang, Yinda Zhang, Yinghao Xu, Yijin Li, Han Zhou, Hujun Bao, Guofeng Zhang, and Zhaopeng Cui. Learning object-compositional neural radiance field for editable scene rendering. In *ICCV*, pages 13779–13788, 2021. 2
- [64] Hao Yang, Lanqing Hong, Aoxue Li, Tianyang Hu, Zhenguo Li, Gim Hee Lee, and Liwei Wang. Contranerf: Generalizable neural radiance fields for synthetic-to-real novel view synthesis via contrastive learning. In *CVPR*, pages 16508–16517, 2023. 2
- [65] Jiawei Yang, Marco Pavone, and Yue Wang. Freenerf: Improving few-shot neural rendering with free frequency regularization. In *CVPR*, pages 8254–8263, 2023. 2, 3
- [66] Yao Yao, Zixin Luo, Shiwei Li, Tian Fang, and Long Quan. Mvsnnet: Depth inference for unstructured multi-view stereo. In *ECCV*, pages 767–783, 2018. 2, 7
- [67] Alex Yu, Vickie Ye, Matthew Tancik, and Angjoo Kanazawa. pixelnerf: Neural radiance fields from one or few images. In *CVPR*, pages 4578–4587, 2021. 2, 3, 4, 6
- [68] Xianggang Yu, Mutian Xu, Yidan Zhang, Haolin Liu, Chongjie Ye, Yushuang Wu, Zizheng Yan, Chenming Zhu, Zhangyang Xiong, Tianyou Liang, et al. Mvimgnet: A large-scale dataset of multi-view images. In *CVPR*, pages 9150–9161, 2023. 1, 2, 6, 7
- [69] Jason Zhang, Gengshan Yang, Shubham Tulsiani, and Deva Ramanan. Ners: Neural reflectance surfaces for sparse-view 3d reconstruction in the wild. *NeurIPS*, 34:29835–29847, 2021. 2
- [70] Jingbo Zhang, Xiaoyu Li, Ziyu Wan, Can Wang, and Jing Liao. Text2nerf: Text-driven 3d scene generation with neural radiance fields. *arXiv preprint arXiv:2305.11588*, 2023. 2
- [71] MI Zhenxing and Dan Xu. Switch-nerf: Learning scene decomposition with mixture of experts for large-scale neural radiance fields. In *ICLR*, 2023. 2
- [72] Tinghui Zhou, Richard Tucker, John Flynn, Graham Fyffe, and Noah Snavely. Stereo magnification: Learning view synthesis using multiplane images. *arXiv preprint arXiv:1805.09817*, 2018. 6
- [73] Zhizhuo Zhou and Shubham Tulsiani. Sparsefusion: Distilling view-conditioned diffusion for 3d reconstruction. In *CVPR*, pages 12588–12597, 2023. 3
- [74] Haidong Zhu, Yuyin Sun, Chi Liu, Lu Xia, Jiajia Luo, Nan Qiao, Ram Nevatia, and Cheng-Hao Kuo. Multimodal neural radiance field. In *ICRA*, pages 9393–9399, 2023. 2
- [75] Haidong Zhu, Zhaoheng Zheng, Wanrong Zheng, and Ram Nevatia. Cat-nerf: Constancy-aware tx2former for dynamic body modeling. In *CVPRW*, pages 6618–6627, 2023. 2
- [76] Yiyu Zhuang, Hao Zhu, Xusen Sun, and Xun Cao. Mofanerf: Morphable facial neural radiance field. In *ECCV*, pages 268–285, 2022. 2
- [77] Dominik Zimny, T Trzciński, and Przemysław Spurek. Points2nerf: Generating neural radiance fields from 3d point cloud. *arXiv preprint arXiv:2206.01290*, 2022. 3